SPECTRAL COLLOCATION ON TRIANGULAR ELEMENTS

by

Wilhelm Heinrichs

Universität GH Essen, Ingenieurmathematik (FB 10)
Universitätsstr. 3, D-45117 Essen, Germany

Abstract

We consider the Poisson problem on a segment of the unit disc and on triangles. On the segment we transform the Poisson problem by means of polar coordinates. In these new coordinates we have a problem in a rectangle which can easily be mapped onto the square. Here standard Chebyshev collocation techniques can be applied. Then the segment is mapped onto a triangle where the same spectral scheme may be used. By numerical tests we observed the expected high spectral accuracy. Due to the corner singularity a singular behaviour of the solution can be expected. Here we improved the accuracy by auxiliary mapping techniques. Further it is shown that finite difference preconditioning can be successfully applied in order to construct an efficient iterative solver. Finally a domain decomposition technique is applied to the patching of a rectangular and a triangular element.

AMS(MOS) classification: 65N35

Keywords: spectral, collocation, triangles, auxiliary mapping, preconditioning, domain decomposition.

Tables: 15

Figures: 5

1 Introduction

It is well known that spectral collocation schemes can be successfully applied to elliptic problems in rectangular domains. For smooth solutions the high (exponential) spectral accuracy can be achieved. Here we are interested in spectral collocation on triangular elements. For the $p-$ and the $h-p-$version of the finite element method the optimal nodes for quadrature are investigated by Babuška et al. [1], [3]-[5]. These techniques are limited to finite element discretizations. For spectral schemes it is not a priori clear which collocation nodes have to be chosen. It is not possible to employ the standard Gauss-Lobatto nodes in both directions. Hesthaven [12] presented optimal nodal sets based on an electrostatic interpretation of the nodes. Gottlieb and Hesthaven [9] studied stable spectral schemes for conservation laws on triangles with unstructured grids. Sherwin and Karniadakis [14] proposed an unstructured spectral element method on triangular and tetrahedral subdomains where a special spectral basis (see Dubiner [7]) has been employed. Wingate et al. [15], [16], [17] consider spectral element methods on triangles for geophysical fluid dynamics problems and the shallow water equations. Here special function spaces for triangular spectral elements are introduced. Modifications of the classical modified Dubiner's basis are proposed, called 'interior-orthogonal' basis. The new basis retains the most important properties of the Dubiner's basis, but gives a weight matrix which is simpler. Here we follow a completely different approach where the standard spectral Cheyshev basis is used. We propose a mapping technique where the Poisson problem is first mapped onto a segment of the unit disc. For this purpose polar coordinates are used. In polar coordinates we have a rectangular domain in $(r, \theta) \in \Omega_{\theta_1} = (0, 1) \times (0, \theta_1)$ for $0 < \theta_1 \leq 2\pi$. Then for $0 < \theta_1 < \pi$ the circular boundary of the segment is mapped onto an edge of the triangle. This means that now r depends on θ, i.e., $r = r(\theta)$. In Ω_{θ_1} we discretize by means of the standard Chebyshev collocation scheme. Hence we approximate by Chebyshev polynomials and collocation is performed at the Chebyshev Gauss-Lobatto nodes in (r, θ). Homogeneous Dirichlet boundary conditions are enforced on the boundary $\partial\Omega_{\theta_1}$. It is numerically shown that for smooth solutions the high spectral accuracy can be achieved. However, the geometric singularity often gives rise to singular solutions. Here we investigated auxiliary mapping techniques to smooth the singularity. This approach was intensively studied by Pathria and Karniadakis [13] for spectral elements. The problem is mapped from Ω_{θ_1} to Ω_π so that the corner is eliminated. But now the singularity is caused by the singular behaviour of the right hand side. Nevertheless for $\theta_1 > \frac{\pi}{\sqrt{2}}$ the singularity is now much weaker which leads to an improvement in accuracy. This is confirmed by numerical experiments. Finally we study finite difference preconditioning. It is shown that the condition number becomes independent of N. This can be used in constructing efficient iterative solvers. For more complicated geometries where rectangular and triangular subdomains match we propose a domain decomposition technique. Here a Dirichlet-Neumann interface relaxation (see Funaro, Quarteroni and Zanolli [8]) is iterated until continuity of normal derivatives is achieved. Numerical results demonstrate the efficiency of our treatment.

2 Transformation of triangular elements

We consider the Poisson problem in a segment, i.e.,

$$\begin{aligned} \Delta u &= f \ in \ \Omega_{\theta_1}, & (1)\\ u &= 0 \ on \ \partial\Omega_{\theta_1} & (2) \end{aligned}$$

where f denotes a given force and

$$\Omega_{\theta_1} = \{(x,y) = r(\cos\theta, \sin\theta) : \ 0 < r < 1, \ 0 < \theta < \theta_1\}$$

denotes a segment with angle θ_1. As usual $\partial\Omega_{\theta_1}$ denotes the boundary of Ω_{θ_1}.
In polar coordinates the Poisson problem can equivalently be written as:

$$\begin{aligned} r^2 u_{rr} + r u_r + u_{\theta\theta} &= r^2 f \ in \ Q_{\theta_1}, & (3)\\ u &= 0 \ on \ \partial Q_{\theta_1} & (4) \end{aligned}$$

where

$$Q_{\theta_1} = \{(r,\theta) : \ 0 < r < 1, \ 0 < \theta < \theta_1\}.$$

Here we multiplied the transformed Laplace operator by r^2. As we see later this representation has advantages for preconditioning.
Further we are interested in the Poisson problem on triangular elements given by

$$T_{\theta_1} = \{(x,y) = \frac{r}{\cos\theta + t_1 \sin\theta}(\cos\theta, \sin\theta) : \ 0 < r < 1, \ 0 < \theta < \theta_1\}$$

where

$$t_1 \;=\; \tan\frac{\theta_1}{2}.$$

T_{θ_1} results from Ω_{θ_1} by mapping the circular boundary to an edge of the triangle. This is accomplished by the mapping:

$$r \;\rightarrow\; r(\theta) = \frac{r}{\cos\theta + t_1 \sin\theta}.$$

Hereby we obtain the third edge which is in $x, y-$coordinates given by

$$x \;+\; t_1 y = 1.$$

For instance, for $\theta_1 = \frac{\pi}{2}$ we obtain $t_1 = 1$ and the straight line $y = 1 - x$. For a fixed radius $r, 0 < r < 1$ the transform is given by $x + t_1 y = r$ and $\tan\theta = \frac{y}{x}$. This yields:

$$\begin{aligned}
u_x &= u_r \;-\; \frac{y}{x^2+y^2} u_\theta, \\
u_{xx} &= u_{rr} \;-\; \frac{2y}{x^2+y^2} u_{r\theta} \;+\; \frac{y^2}{(x^2+y^2)^2} u_{\theta\theta} \;+\; \frac{2xy}{(x^2+y^2)^2} u_\theta
\end{aligned}$$

and

$$\begin{aligned}
u_y &= t_1 u_r \;+\; \frac{x}{x^2+y^2} u_\theta, \\
u_{yy} &= t_1^2 u_{rr} \;+\; 2t_1 \frac{x}{x^2+y^2} u_{r\theta} \;+\; \frac{x^2}{(x^2+y^2)^2} u_{\theta\theta} \;-\; \frac{2xy}{(x^2+y^2)^2} u_\theta.
\end{aligned}$$

Hence the Poisson problem in T_{θ_1} can equivalently be written as:

$$(1+t_1^2)(x^2+y^2) u_{rr} \;+\; 2(t_1 x - y) u_{r\theta} \;+\; u_{\theta\theta} \;=\; (x^2+y^2) f \;\; in \;\; T_{\theta_1} \quad (5)$$

$$u \;=\; 0 \;\; on \;\; \partial T_{\theta_1} \quad (6)$$

or

$$\begin{aligned}
\frac{1+t_1^2}{(\cos\theta + t_1\sin\theta)^2} r^2 u_{rr} \;+\; 2\frac{t_1\cos\theta - \sin\theta}{\cos\theta + t_1 \sin\theta} r u_{r\theta} \;+\; u_{\theta\theta} &= \\
&= \frac{r^2}{(\cos\theta + t_1\sin\theta)^2} f \quad in \;\; Q_{\theta_1} \\
u &= 0 \;\; on \;\; \partial Q_{\theta_1}.
\end{aligned}$$

Therefore in both cases we are able to transform the Poisson problem onto the rectangle Q_{θ_1}.

3 Spectral discretization

For the spectral approximation we use a standard Chebyshev collocation scheme. It is defined on the Chebyshev Gauss-Lobatto nodes given by

$$(s_i, t_j) = (\cos\frac{i\pi}{N}, \cos\frac{j\pi}{N}), \; i, j = 0, \ldots, N.$$

Hence Fast Fourier Transforms (FFTs) are available for the efficient evaluation of spectral derivatives. In the two-dimensional case they can be evaluated in $O(N^2 \log N)$ arithmetic operations. These nodes are mapped on $(r, \theta) \in (0,1) \times (0, \theta_1)$ by the linear transform:

$$r_i = \frac{1}{2}(s_i + 1), \quad \theta_j = \frac{\theta_1}{2}(t_j + 1).$$

By using these nodes in (r, θ) we plot for $N = 16$ the collocation nodes on Ω_{θ_1} for $\theta_1 = \frac{\pi}{2}, \pi, \frac{3}{2}\pi$ and T_{θ_1} for $\theta_1 = \frac{\pi}{2}$ in the figures 1-3, 4. As expected the nodes are clustering near the corner $r = 0$. Now we present the Chebyshev collocation scheme in the (r, θ) coordinate system. As usual we employ a Chebyshev approximation $u_N \in \mathrm{IP}_N^0$ where

$$\mathrm{IP}_N^0 = \{p : p \; polynomial \; of \; degree \; \leq N \; in \; s, t \; vanishing \; on \; the \; boundary\}.$$

u_N can be written as

$$u_N = \sum_{m,n=0}^{N} a_{m,n} T_m(s) T_n(t), \; a_{m,n} \in \mathrm{IR},$$

where $T_m(s) = \cos m \arccos s$ denotes the mth Chebyshev polynomial. The boundary conditions are automatically fulfilled and we require at the $(N-1)^2$ collocation nodes:

$$\left(r^2 u_{rr} \; + \; r u_r \; + \; u_{\theta\theta}\right)(r_i, \theta_j) = r_i^2 f(r_i, \theta_j) \; for \; i, j = 1, \ldots, N-1.$$

Similar collocation conditions are required for equation (5). The spectral approximation is now uniquely determined. The occuring derivatives $u_{rr}, u_r, u_{\theta\theta}$ can be spectrally evaluated by using the standard Chebyshev collocation derivatives in the (s,t)-coordinate system. Obviously, we obtain

$$\begin{aligned} u_r &= 2u_s, \; u_{rr} = 4u_{ss}, \\ u_\theta &= \frac{2}{\theta_1} u_t, \; u_{\theta\theta} = \frac{4}{\theta_1^2} u_{tt}, \; u_{r\theta} = \frac{4}{\theta_1} u_{st}. \end{aligned}$$

The spectral collocation derivative is given by $D_N = (d_{i,j})_{i,j=0,\ldots,N}$ (see Canuto et al. [2]) where

$$d_{i,j} = \begin{cases} \frac{c_i}{c_j}\frac{(-1)^{i+j}}{s_i-s_j}, & i \neq j \\ -\frac{s_j}{2(1-s_j^2)}, & 1 \leq i = j \leq N-1 \\ \frac{2N^2+1}{6}, & i = j = 0 \\ -\frac{2N^2+1}{6}, & i = j = N. \end{cases}$$

and

$$c_i = \begin{cases} 2, & i \in \{0, N\} \\ 1, & i = 1, \ldots, N-1. \end{cases}$$

Partial derivatives can be obtained by means of tensor product representation ($\otimes$) with the identity matrix I_N, i.e.,

$$\begin{aligned} \frac{\partial}{\partial r} &\cong 2\left(D_N \otimes I_N\right), \ \frac{\partial^2}{\partial r^2} \cong 4\left(D_N^2 \otimes I_N\right) \\ \frac{\partial}{\partial \theta} &\cong \frac{2}{\theta_1}\left(I_N \otimes D_N\right), \ \frac{\partial^2}{\partial \theta^2} \cong \frac{4}{\theta_1^2}\left(I_N \otimes D_N^2\right) \\ \frac{\partial^2}{\partial r \partial \theta} &\cong \frac{4}{\theta_1}\left(D_N \otimes D_N\right). \end{aligned}$$

Now the spectral operators are well defined. For these spectral discretizations we expect the high spectral accuracy. For smooth (analytical) solutions exponential convergence can be observed. We tested the accuracy for the following two examples where the exact solutions (in the (x, y)-coordinate system) are given by

$$u(x,y) = xy\left(e^{x^2+y^2} - e\right), \ \theta_1 = \frac{\pi}{2} \tag{7}$$

for problem (3) and

$$u(x,y) = xy\left(e^{x+y} - e\right), \ \theta_1 = \frac{\pi}{2} \tag{8}$$

for problem (5). We calculated the discrete L^2-error $E2$ which is given by $E2 = ||u - u_N||$. From the numerical results in the tables I,II we observe the exponential decay of the error. For example (7) the rounding error accuracy is already reached for $N = 16$. This is due to the fact that the exponent $x^2 + y^2 = r^2$ is independent of θ.

N	$E2$
4	$1.94 \cdot 10^{-3}$
8	$6.62 \cdot 10^{-7}$
16	$7.82 \cdot 10^{-15}$
32	$5.79 \cdot 10^{-15}$

Table I. Results for example (7)

N	$E2$
4	$1.89 \cdot 10^{-4}$
8	$8.85 \cdot 10^{-7}$
16	$1.84 \cdot 10^{-11}$
32	$1.78 \cdot 10^{-16}$

Table II. Results for example (8)

From the numerical results we observe an uniform resolution over the whole domain. Clearly, the collocation points are clustering near the corner but there is nearly no difference in the error distribution. The nodes are optimal since the original problem on the triangular element is transformed onto an elliptic problem on the square. On the square it is well known that Gauss-Lobatto nodes are optimal. A precise convergence analysis is quite difficult because of the singular coefficients in the differential operator. But from the eigenvalue computations in section 5 it becomes clear that the spectral operator is numerically elliptic.

4 Singular solutions and auxiliary mappings

The geometric singularity (corner in $r = 0$) often gives rise to singular solutions. The irregularity is due to the fact that the differential equation and the boundary conditions are not compatible. This usually leads to a singularity in the corner. The accuracy of the spectral method is then degraded and there is no significant advantage over low-order finite difference or finite element methods. It is possible, however, to use a priori information about the behaviour of the singularity in constructing improved schemes. This has been accomplished by using

- supplementary singular basis functions,
- conformal maps to smooth the singularity,
- domain decomposition techniques or adaptive refinement.

Here we are concerned with auxiliary mappings to smooth the singularity. This technique was already investigated by Pathria and Karniadakis [13] for the spectral element method. For certain simple cases, the problem is transformed to a new coordinate system where the solution is analytic, and exponential convergence is recovered. Even when this is not possible, the singularity is usually much weaker after mapping, so that other treatments are more effective in the new coordinate system. Such a singularity occurs if for instance $f \equiv -1$, i.e.,

$$\begin{aligned} -\Delta u &= 1 \; in \; \Omega_{\theta_1}, \\ u &= 0 \; on \; \partial\Omega_{\theta_1}. \end{aligned}$$

We evaluated u_N in $r = \frac{1}{2}$, $\theta = \frac{\theta_1}{2}$. The computation was performed for $N = 4, 8, 16, 32$ and $\theta_1 = \frac{\pi}{2}, \pi, \frac{3}{2}\pi$. Since the exact solution is not known we compared the values with u_N for $N = 36$. ER denotes the error compared to this value. In the tables III, IV, V we present the numerical results for $\theta_1 = \frac{\pi}{2}, \pi, \frac{3}{2}\pi$.

N	ER
4	$6.30 \cdot 10^{-5}$
8	$2.08 \cdot 10^{-6}$
16	$4.36 \cdot 10^{-8}$
32	$3.81 \cdot 10^{-10}$

Table III. Results for $\theta_1 = \frac{\pi}{2}$

N	ER
4	$6.05 \cdot 10^{-4}$
8	$3.13 \cdot 10^{-6}$
16	$1.01 \cdot 10^{-9}$
32	$1.85 \cdot 10^{-15}$

Table IV. Results for $\theta_1 = \pi$

N	ER
4	$1.87 \cdot 10^{-3}$
8	$1.06 \cdot 10^{-4}$
16	$1.37 \cdot 10^{-5}$
32	$6.11 \cdot 10^{-7}$

Table V. Results for $\theta_1 = \frac{3}{2}\pi$

Only for $\theta_1 = \pi$ we observe spectral accuracy. In the other two cases there is no exponential convergence due to the singular behaviour of the solution. For $\theta_1 = \alpha\pi$ it is shown (see [13]) that mapping is recommended for $\alpha > \frac{1}{\sqrt{2}}$. Hence for $\theta_1 = \frac{3}{2}\pi$ auxiliary mapping leads to an improved accuracy. For $\theta_1 = \frac{\pi}{2}$ there is no improvement. The mapping introduces new coordinates

$$\rho = r^{\frac{1}{\alpha}},\ \sigma = \frac{\theta}{\alpha}\ \ for\ \theta_1 = \alpha\pi.$$

Hence Q_{θ_1} is mapped onto Q_π where the geometric singularity has disappeared. It is easily seen ([13]) that equation (3) is equivalent to

$$\rho^2 u_{\rho\rho} + \rho u_\rho + u_{\theta\theta} = \alpha^2 \rho^{2\alpha} f\ in\ Q_\pi. \tag{9}$$

Compared to (3) there is only a change in the right hand side which now leads the singular behaviour. There is no singularity due to geometry. Typical error estimates in the H^1-norm are presented in [13]:

- without mapping:

$$||u - u_N|| \leq CN^{-\frac{2}{\alpha}-\epsilon},\ C > 0$$

- with mapping:

$$||u - u_N|| \leq CN^{-4\alpha-\epsilon},\ C > 0$$

for any $\epsilon > 0$. Hence for $\alpha = \frac{3}{2}$ it is recommended to use mapping with an error decay proportional to N^{-6} instead of $N^{-\frac{4}{3}}$ without mapping. For $\alpha = \frac{1}{2}$ the mapping technique leads to somewhat worse results. Without mapping the error decay is proportional to N^{-4}. These theoretical predictions were fully confirmed by the numerical results presented in the tables VI, VII.

N	ER
4	$7.54{\cdot}10^{-4}$
8	$3.67{\cdot}10^{-5}$
16	$2.50{\cdot}10^{-6}$
32	$6.36{\cdot}10^{-8}$

Table VI. $\theta_1 = \frac{\pi}{2}$ with mapping

N	ER
4	$8.56{\cdot}10^{-4}$
8	$6.96{\cdot}10^{-6}$
16	$1.47{\cdot}10^{-9}$
32	$1.75{\cdot}10^{-12}$

Table VII. $\theta_1 = \frac{3}{2}\pi$ with mapping

Finally, we consider a non-smooth example where the right hand side f is discontinuous. We consider equations (3), (4) with $\theta_1 = \frac{\pi}{2}$. The function f is now defined by

$$f \equiv \begin{cases} -1, \; x+y<1, \\ \;\;0 \;, \; x+y \geq 1. \end{cases} \tag{10}$$

Hence f has a discontinuity along the axes $x+y=1$. Since now the solution is no more smooth no high accuracy can be expected. From the numerical results in table VIII it can be observed that a first order method results. Here no higher accuracy than for finite difference or finite elements can be achieved.

N	ER
4	$6.32{\cdot}10^{-3}$
8	$1.81{\cdot}10^{-3}$
16	$9.56{\cdot}10^{-4}$
32	$4.04{\cdot}10^{-4}$

Table VIII. Results for example (10).

5 Preconditioning

First, we were interested in the eigenspectrum of the first derivative operators. For the standard spectral schemes (see [2]) it is well known that the largest eigenvalues scale as $O(N^2)$. For reasons of symmetry the eigenvalues of $\frac{\partial}{\partial x}$ and $\frac{\partial}{\partial y}$ are the same. On Ω_{θ_1} we obtain

$$\begin{aligned} u_x &= \cos\theta u_r - \frac{\sin\theta}{r} u_\theta, \\ u_y &= \sin\theta u_r + \frac{\cos\theta}{r} u_\theta. \end{aligned}$$

On T_{θ_1} we have

$$\begin{aligned} u_x &= u_r - \frac{\cos\theta + t_1\sin\theta}{r}\sin\theta u_\theta, \\ u_y &= t_1 u_r + \frac{\cos\theta + t_1\sin\theta}{r}\cos\theta u_\theta. \end{aligned}$$

We fix $\theta_1 = \frac{\pi}{2}$ and calculated the absolutely maximal eigenvalues λ_{max} for $N = 4, 8, 16, 32$. In the tables IX, X we present the numerical results on $\Omega_{\theta_1}, T_{\theta_1}$ for $\theta_1 = \frac{\pi}{2}$. On Ω_{θ_1} the maximal eigenvalues seem to behave as $O(N^3)$ whereas on T_{θ_1} as $O(N^2)$.

N	λ_{max}	λ_{max}/N^3
4	$1.19 \cdot 10^1$	0.19
8	$2.01 \cdot 10^1$	0.39
16	$3.08 \cdot 10^3$	0.75
32	$4.84 \cdot 10^4$	1.48

Table IX. λ_{max} for $\frac{\partial}{\partial x}, \frac{\partial}{\partial y}$ on $\Omega_{\theta_1}, \theta_1 = \frac{\pi}{2}$.

N	λ_{max}	λ_{max}/N^2
4	$4.00 \cdot 10^0$	0.25
8	$1.25 \cdot 10^1$	0.20
16	$4.70 \cdot 10^1$	0.18
32	$1.83 \cdot 10^2$	0.18

Table X. λ_{max} for $\frac{\partial}{\partial x}, \frac{\partial}{\partial y}$ on $T_{\theta_1}, \theta_1 = \frac{\pi}{2}$.

Further we consider finite difference preconditioning for the problems (3) and (5). We fix $\theta_1 = \frac{\pi}{2}$. By numerical tests we found that it is better to work with the equations multiplied by r^2. Another good choice for preconditionig are bilinear finite elements as proposed by Deville and Mund [6]. We have more experience with finite differences. Let w denote a one-dimensional function. The finite difference approximations for the first and second derivative are given by

$$\begin{aligned} w'(s_j) &= 0.5\left(-\gamma_{j-1} w(s_{j-1}) - (\gamma_j - \gamma_{j-1}) w(s_j) + \gamma_j w(s_{j+1})\right), \\ w''(s_j) &= 2\delta_j \left(\gamma_{j-1} w(s_{j-1}) - (\gamma_j + \gamma_{j-1}) w(s_j) + \gamma_j w(s_{j+1})\right) \end{aligned}$$

where

$$\begin{aligned} \delta_j &= \frac{1}{s_{j+1} - s_{j-1}}, \\ \gamma_j &= \frac{1}{s_{j+1} - s_j}, \quad j = 1, \ldots, N-1. \end{aligned}$$

The finite difference discretization of the equations (3), (5) can now be derived by tensor product representation. In the tables XI, XII we present the absolute value of the minimal and maximal eigenvalues λ_{min} and λ_{max} for the spectral operators of the equations (3), (5). The quantity

$$cond = \frac{\lambda_{max}}{\lambda_{min}}$$

yields a reasonable approximation of the condition number.

N	λ_{min}	λ_{max}	$cond$
4	4.49	$7.59 \cdot 10^1$	$1.69 \cdot 10^1$
8	4.26	$1.11 \cdot 10^3$	$2.59 \cdot 10^2$
16	4.16	$1.75 \cdot 10^4$	$4.20 \cdot 10^3$
32	4.12	$2.79 \cdot 10^7$	$6.78 \cdot 10^6$

Table XI. Results for the spectral operator (3).

N	λ_{min}	λ_{max}	$cond$
4	5.10	$1.15 \cdot 10^2$	$2.26 \cdot 10^1$
8	4.58	$1.89 \cdot 10^3$	$4.15 \cdot 10^2$
16	4.39	$3.07 \cdot 10^4$	$7.00 \cdot 10^3$
32	4.29	$4.93 \cdot 10^5$	$1.15 \cdot 10^5$

Table XII. Results for the spectral operator (5).

In the tables XIII, XIV we present the corresponding results for the preconditioned spectral operators. As expected the condition number is dramatically reduced by preconditioning. It is only slightly increasing in N. This is the typical behaviour which was already observed for the spectral Laplacian on rectangular domains (see [10], [11]).

N	λ_{min}	λ_{max}	$cond$
4	0.63	1.73	2.75
8	0.62	2.13	3.44
16	0.62	2.30	3.73
32	0.62	2.39	3.87

Table XIII. Results for the preconditioned operator (3).

N	λ_{min}	λ_{max}	$cond$
4	0.99	1.71	1.73
8	0.99	2.12	2.13
16	0.80	2.41	3.01
32	0.66	2.83	4.31

Table XIV. Results for the preconditioned operator (5).

6 Domain decomposition

Here we consider the patching of a rectangle with a triangle. We solve the problem

$$\begin{aligned} \Delta u &= f \ in \ \Omega_h, && (11) \\ u &= g \ on \ \partial\Omega_h && (12) \end{aligned}$$

where f, g denote given data and

$$\Omega_h = T_{\theta_1} \cup R, \quad R = (0,1) \times (-1, 0].$$

We fix $\theta_1 = \frac{\pi}{3}$ so that Ω_h has the shape of a house (see figure 5). On the interface $\Gamma = (0,1)$ we use an interface relaxation procedure as proposed by Funaro, Quarteroni and Zanolli [8]. Here a sequence of Dirichlet-Neumann problems is iterated till convergence. Continuity of normal derivatives at the interfaces are enforced. The iteration proceeds until C^1 continuity is achieved to some prescribed tolerance (10^{-14} in our experiments). The Poisson problem is solved on each subdomain T_{θ_1} and R. We start with $u_1^0 = u_2^0 \equiv 0$ and then for $m = 1, 2, \ldots$ iterate as follows:

$$\begin{aligned} \Delta u_1^m &= f \ in \ T_{\theta_1}, \\ u_1^m &= g \ on \ \partial T_{\theta_1} - \Gamma, \\ u_1^m &= \delta^m u_2^{m-1} + (1 - \delta^m) u_1^{m-1} \ on \ \Gamma \end{aligned}$$

and

$$\begin{aligned} \Delta u_2^m &= f \ in \ R, \\ u_2^m &= g \ on \ \partial R - \Gamma, \\ \frac{\partial u_2^m}{\partial \nu} &= \frac{\partial u_1^m}{\partial \nu} \ on \ \Gamma, \ \nu \ outer \ normal. \end{aligned}$$

δ^m denotes the relaxation parameter which is chosen dynamically in order to accelerate the convergence. Usually it is the unique real minimizer of the error between successive iterates and is computed as:

$$\delta^m = \frac{(e_1^m, e_1^m - e_2^m)}{||e_1^m - e_2^m||^2}$$

where $(\cdot,\cdot)$ denotes the discrete L^2 inner product and

$$e_i^m = u_i^m - u_i^{m-1},\ i = 1,2$$

is the difference between two iterates on the relevant subdomain. This iteration proceeds till some prescribed tolerance along the interface (here 10^{-14}). In table XV we present the numerical results for an example where the exact solution with nonhomogeneous boundary conditions is given by

$$u(x,y) = \sin\left(3\pi x + \frac{\pi}{4}\right)\sin\left(3\pi y + \frac{\pi}{4}\right),\quad \theta_1 = \frac{\pi}{3}. \tag{13}$$

It denotes the number of interface relaxations which are necessary till convergence. Afterwards the discrete L^2 errors $E2_1, E2_2$ on the subdomains $T_{\frac{\pi}{3}}, R$ are calculated. From the numerical results we once more observe exponential convergence of the patched spectral scheme. Hence we also found a highly accurate method for domains with five corners. Clearly, these techniques can be generalized to domains with an odd number of corners.

N	It	$E2_1$	$E2_2$
4	11	$5.89 \cdot 10^{-1}$	$3.80 \cdot 10^{-1}$
8	18	$5.49 \cdot 10^{-3}$	$3.59 \cdot 10^{-3}$
16	25	$5.37 \cdot 10^{-8}$	$1.60 \cdot 10^{-8}$
32	36	$8.44 \cdot 10^{-14}$	$4.95 \cdot 10^{-14}$

Table XV. Results for example (13).

7 Summary

By using polar coordinates triangular elements are mapped on rectangular domains where standard spectral collocation schemes are available. Here a Chebychev collocation method with Gauss-Labatto nodes in the polar coordinates is employed. Both for smooth and singular solutions the expected high spectral accuracy is achieved. The accuracy is determined only by the smootheness of the solution. More complicated geometries consisting of triangular and rectangular subdomains can be treated efficiently by a domain decomposition approach and patching techniques. Here a Dirichlet-Neumann relaxation is iterated until the continuity of the normal derivatives on the interfaces is achieved.

References

[1] Babuška, I. and Suri, M.: The p- and h-p version of the finite element method. An overview. Comput. Meth. Appl. Mech. Engrg. **80**, 5-26(1990)

[2] Canuto, C., Hussaini, M.Y., Quarteroni, A., and Zang, T.A.: Spectral Methods in Fluid Dynamics, Springer Series in Computational Physics, Springer-Verlag, Berlin-Heidelberg-New York, 1989

[3] Chen, Q. and Babuška, I.: Approximate optimal points for polynomial interpolation of a real function in an interval and in a triangle. Comp. Meth. Appl. Mech. Engrg. **128**, 405-417(1996)

[4] Chen, Q. and Babuška, I.: The optimal symmetric points for polynomial interpolation of real functions in the tetrahedron. Comp. Meth. Appl. Mech. Engrg. **137**, 89-94(1996)

[5] Chen, Q. and Babuška, I.: Adaptive procedure for approximating functions by continuous piecewise polynomials. Comm. Numer. Meth. Engrg. **12**, 483-495(1996)

[6] Deville, M. and Mund, E.: Chebyshev pseudospectral solution of second-order elliptic equations with finite element preconditioning. J. Comp. Phys. **60**, 517-533(1985)

[7] Dubiner, M.: Spectral methods on triangular and other domains. J. Sci. Comp. **6**, 345 (1991)

[8] Funaro, D., Quarteroni, A., and Zanolli, P.: An iterative procedure with interface relaxation for domain decompositon methods. SIAM J. Numer. Anal. **25**, 1213-1236(1988)

[9] Gottlieb, D. and Hesthaven, J.S.: Stable spectral methods for conservation laws on triangles with unstructured grids. To appear in SIAM J. Numer. Anal. 1998

[10] Heinrichs, W.: Line relaxation for spectral multigrid methods. J. Comp. Phys. **77**, 166-182(1988)

[11] Heinrichs, W.: Multigrid methods for combined finite difference and Fourier problems. J. Comp. Phys. **78**, 424-436(1988)

[12] Hesthaven, J.S.: From electrostatics to almost optimal nodal sets for polynomial interpolation in a simplex. SIAM J. Numer. Anal. **35**, No. 2, 655-676(1998)

[13] Pathria, D. and Karniadakis, G.E.: Spectral element methods for elliptic problems in nonsmooth domains. J. Comp. Phys. **122**, 83-95(1995)

[14] Sherwin, S.J. and Karniadakis, G.E.: Triangular and Tetrahedral spectral elements, *in* Proceedings of the Third International Conference on Spectral and High Order Methods. Houston Journal of Mathematics, A.V. Ilin and L.R. Scott (eds.), Houston, Texas 1996

[15] Wingate, B.A. and Boyd, J.P.: Spectral element methods on triangles for geophysical fluid dynamics problems, *in* Proceedings of the Third International Conference on Spectral and High Order Methods, A.V. Ilin and L.R. Scott (eds.), Houston, Texas 1996

[16] Wingate, B.A. and Taylor, M.A.: The natural function space for triangular spectral elements. SIAM J. Numer. Anal., 1998. Submitted

[17] Wingate, B.A. and Taylor, M.A.: A (Fekete) point triangular spectral element method; application to the shallow water equations. J. Comput. Phys., 1998. Submitted

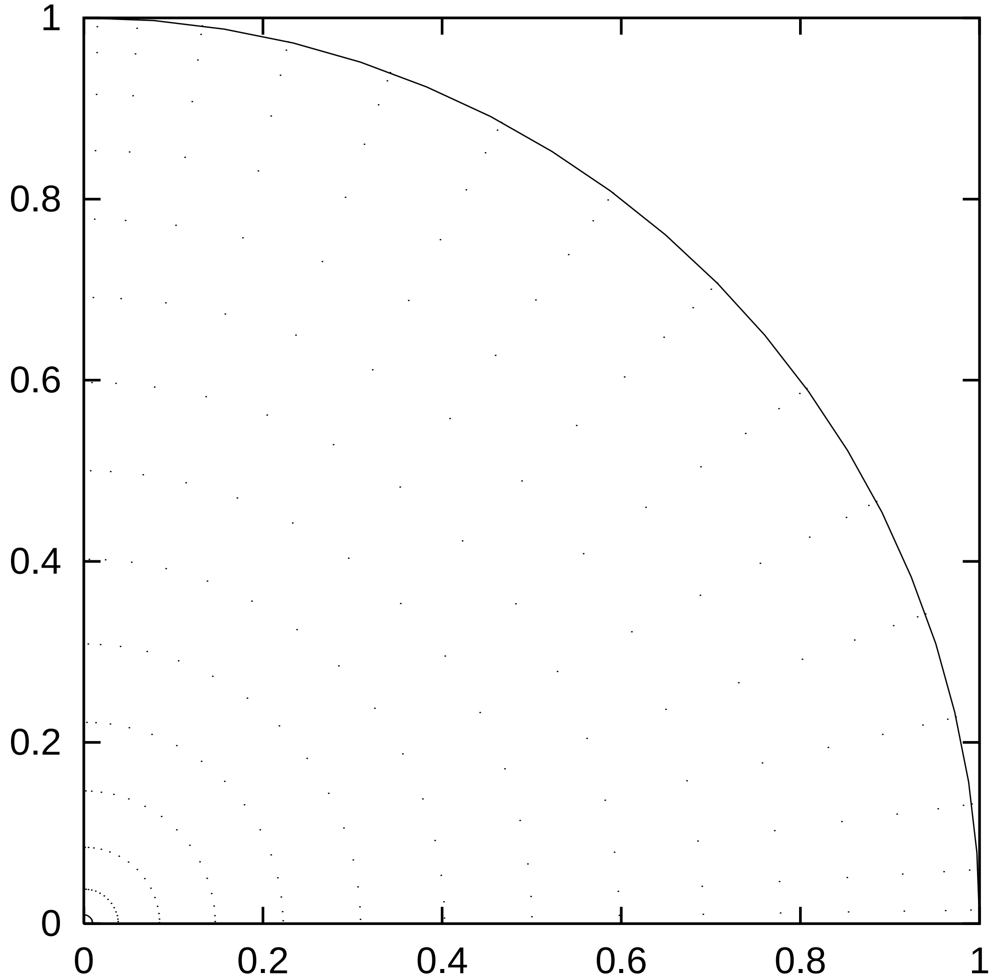

Figure 1. Collocation nodes in $\Omega_{\frac{\pi}{2}}$

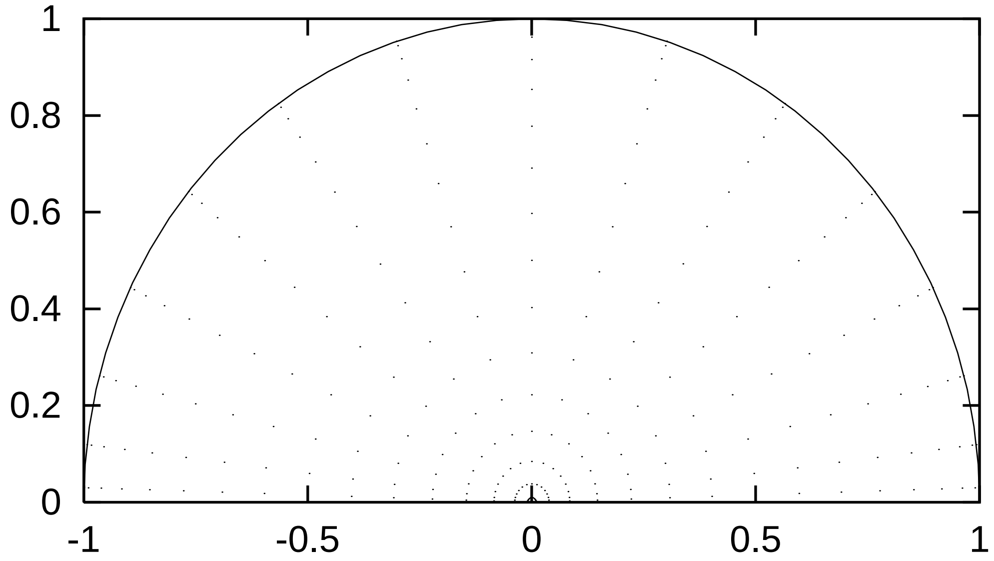

Figure 2. Collocation nodes in Ω_π

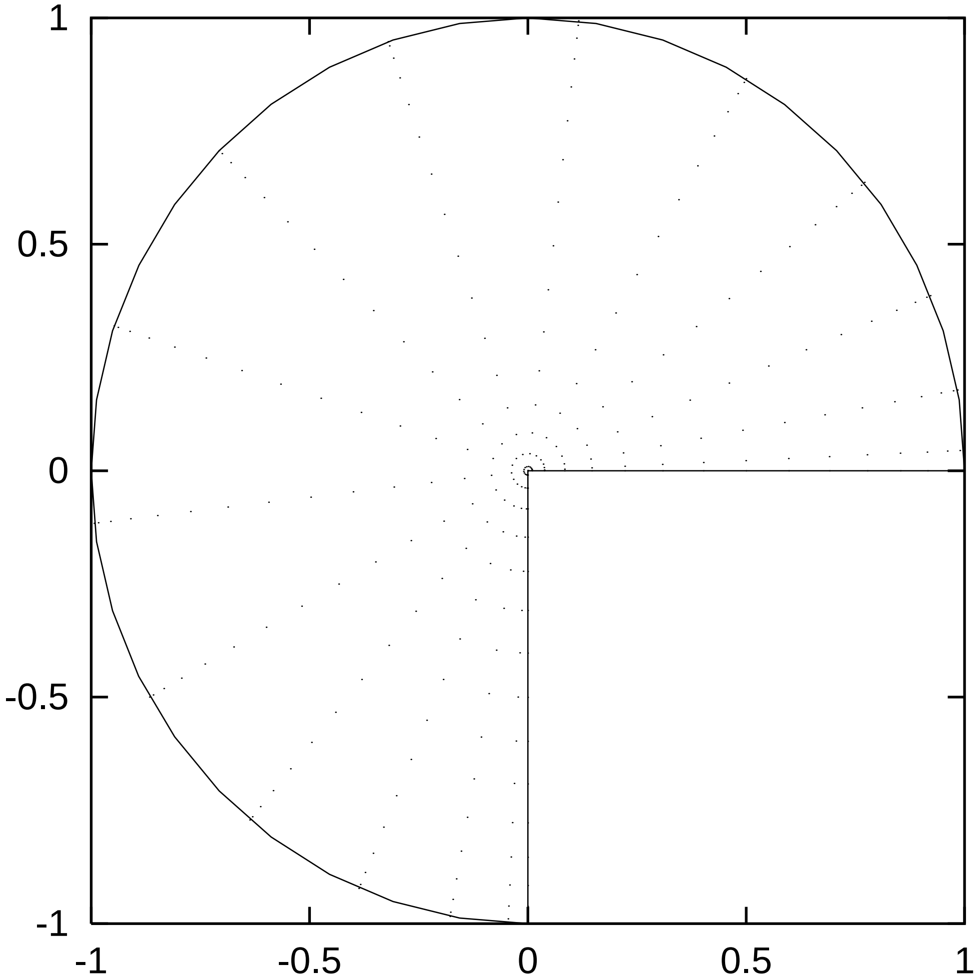

Figure 3. Collocation nodes in $\Omega_{\frac{3\pi}{2}}$

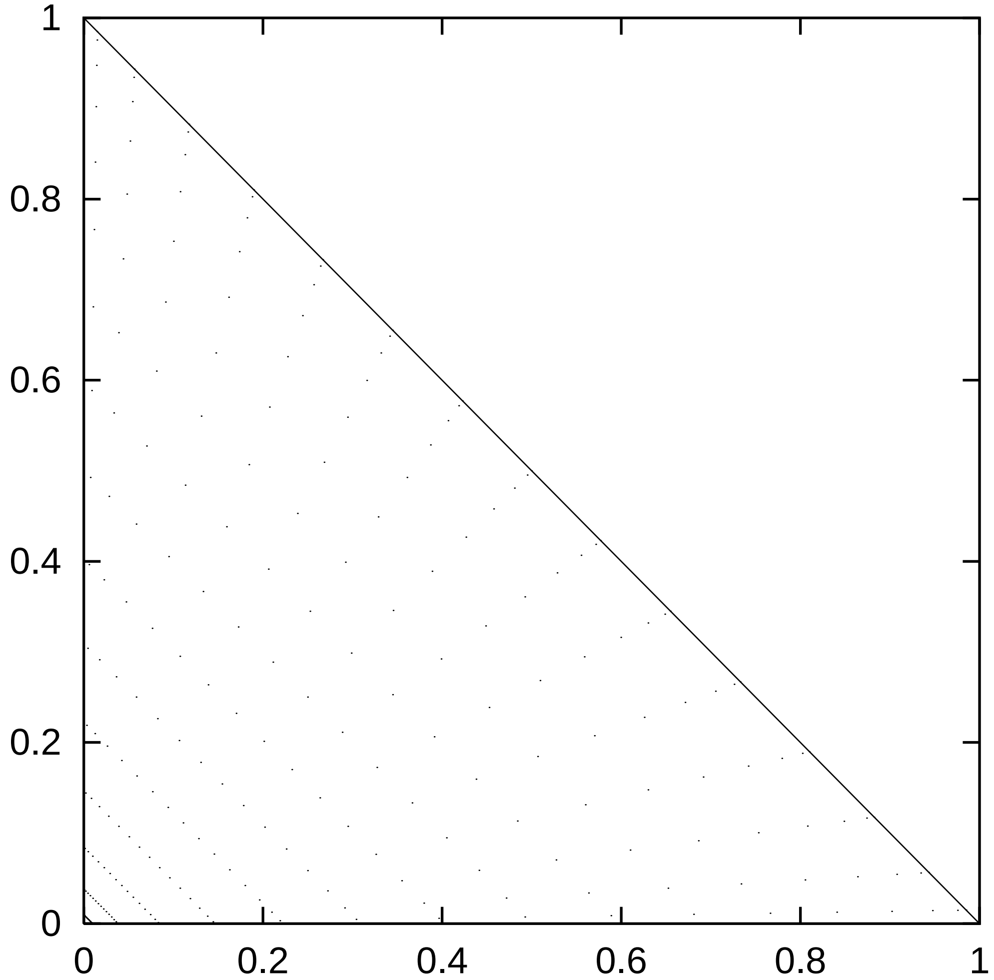

Figure 4. Collocation nodes in $T_{\frac{\pi}{2}}$

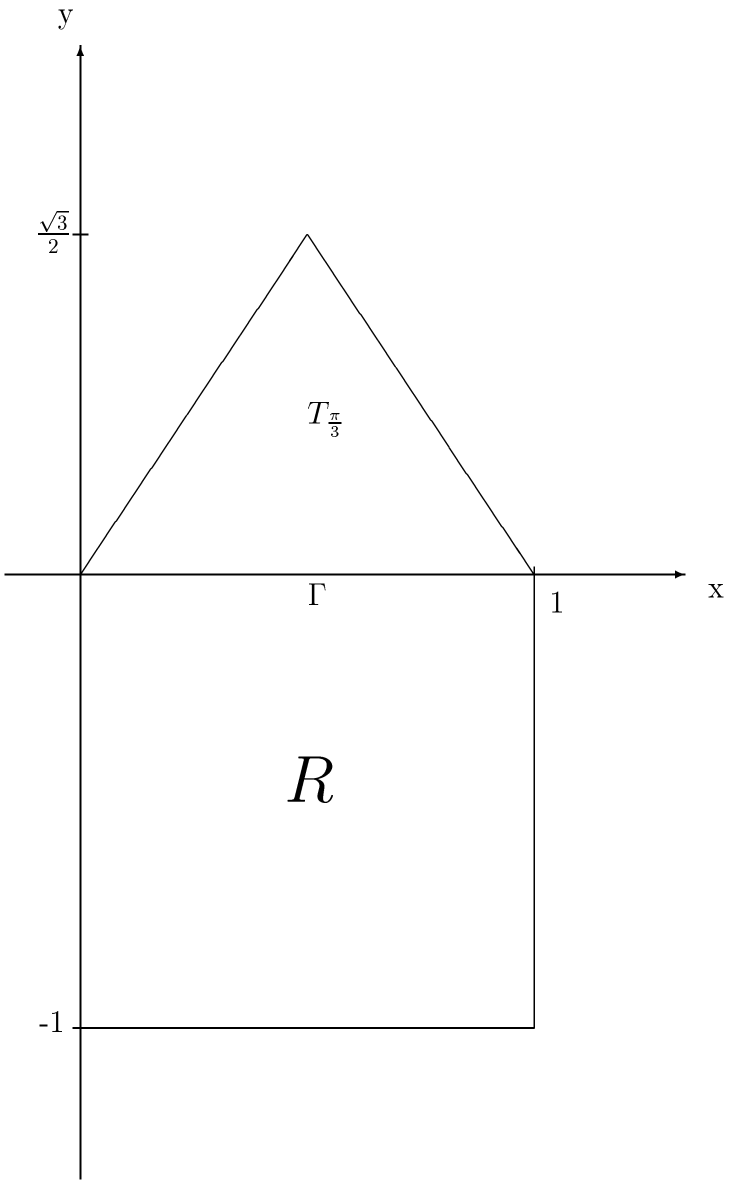

Figure 5. Figure of Ω_h